

# The Anomalous Resonant Frequency Variation of Microwave Superconducting Niobium Cavities Near $T_c$

D. Bafia,<sup>1,\*</sup> A. Grassellino,<sup>1</sup> M. Checchin,<sup>1</sup> J. F. Zasadzinski,<sup>2</sup> and A. Romanenko<sup>1</sup>

<sup>1</sup>*Fermi National Accelerator Laboratory, Batavia, Illinois 60510, USA*

<sup>2</sup>*Department of Physics, Illinois Institute of Technology, Chicago, Illinois 60616, USA*

(Dated: July 8, 2022)

Superconducting radio-frequency (SRF) niobium cavities are the modern means of particle acceleration and an enabling technology for record coherence superconducting quantum systems and ultra-sensitive searches for new physics. Here we report a systematic effect observed on a large set of bulk SRF cavities - an anomalous decrease of the resonant frequency at temperatures just below the superconducting transition temperature - which opens up a new means of understanding the physics behind nitrogen doping and other modern cavity surface treatments relevant for future quality factor and coherence improvements. The magnitude of the frequency change correlates systematically with the near-surface impurity distribution in studied cavities and with the observed  $T_c$  variation. We also present the first demonstration of the coherence peak in the real part of the AC complex conductivity in Nb SRF cavities and show that its magnitude varies with impurity distribution.

Superconducting radio-frequency (SRF) niobium cavities are the record-high quality factor  $Q_0 > 10^{10} - 10^{11}$  man-made resonators that serve as the primary continuous wave accelerating structures in modern particle accelerators [1], longest coherence microwave quantum superconducting systems [2], and an ultra-sensitive platform for dark sector and dark matter candidate searches [3–6].

An important feature of SRF cavities is the dependence of the quality factor on the magnitude of the stored microwave field. Extensive research over the past decades allowed uncovering and mitigating several such field-dependent physical mechanisms in various regimes [1]. The most recent ones include the proximity-coupled niobium nanohydrides [7] and their mitigation by oxygen inward diffusion [8] and two-level systems (TLS) [2, 9].

However, some of the effects remain less understood, most notably the physical mechanism behind the field-dependent *increase* in the quality factor of nitrogen doped [10] cavities. The effect comes from the “BCS” component [11] of the surface resistance [10], and detailed material studies highlighted its dependence on the near-surface interstitial nitrogen concentration and distribution. For the microscopic mechanism, one suggested possibility is the field-driven non-equilibrium redistribution of thermally excited quasiparticles to higher energy levels. Studies on cavities of different frequencies [12] provide support for this possibility. Still, a systematic study of the effect of doping on the quasiparticle lifetimes, number density, and coupling strength in SRF cavities has not been reported yet and is critical for the full understanding of the effect. Furthermore, oxygen diffusion during 120°C baking [13] also leads to a strongly suppressed electron mean free path in the near-surface region [14] - similar to nitrogen doping - but the field-dependent increase in  $Q_0$  is not present. This indicates that different impurities may have a different effect on relevant superconducting properties, another important aspect to be clarified.

While many studies have focused on the quality fac-

tor, cavity resonant frequency provides another valuable avenue for gaining insight into the underlying physical phenomena, as its changes are directly connected to the properties of the superconducting condensate.

The AC complex conductivity  $\sigma = \sigma_1 + i\sigma_2$  enables further insight on quasiparticles and superconducting carriers. For frequencies far below the superconducting gap ( $\hbar\omega \ll \Delta$ ),  $\sigma_1$  exhibits the so-called coherence peak, a non-monotonic dependence of the quasiparticle conductivity with temperature that arises due to coherence factors in BCS theory [15] and is analogous to the Hebel-Slichter peak in nuclear spin relaxation [16]. However, until now, this coherence peak has not been reported in Nb SRF cavities.

In this article, we present a systematic study of a large number ( $>40$ ) of state-of-the-art bulk niobium SRF cavities revealing an anomalous decrease (dip) in the cavity resonant frequency at temperatures just below  $T_c$  in nitrogen doped cavities as well as other (non-dip) characteristic temperature dependencies uniquely corresponding to each of the other explored surface treatments. We also report the first measurement of the coherence peak in bulk niobium SRF cavities. Fits of the complex conductivity with a phenomenological model incorporating Dynes description show that the dip phenomenon is present when the level of inelastic scattering is low ( $\Gamma/\Delta_0 = 0.0058$ ) and the average superconducting gap is large ( $\Delta_0 = 1.6$  meV). These values are in good agreement with those observed in previous point contact tunneling studies on similar samples.

We employed a large set of bulk niobium SRF cavities of TESLA [17] elliptical shape for our studies. The design resonant frequencies of these cavities varied from 650 MHz to 3.9 GHz, which allowed probing the low frequency ( $\hbar\omega \ll \Delta$ ) limit of Nb. All the cavities went through a bulk electropolishing of about 120  $\mu\text{m}$  material removal as a first step followed by different modern surface treatments on subsets of multiple cavities in each.

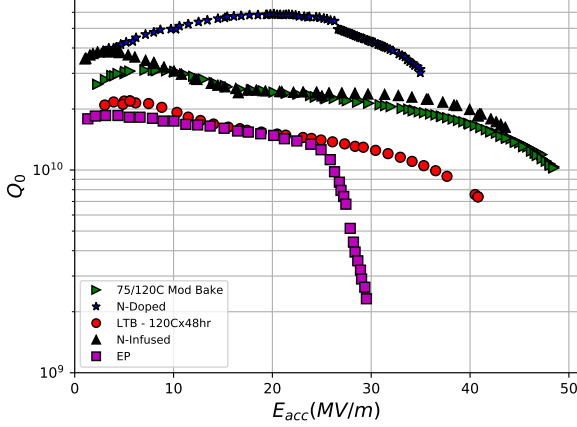


FIG. 1. Characteristic CW RF test results at 2 K of TESLA-shaped 1.3 GHz cavities subjected to surface treatments used in this study.

The treatments investigated included hydrogen degassing at 800°C followed by additional 40  $\mu\text{m}$  electropolishing, nitrogen doping [10] with varying dopant concentrations, nitrogen infusion [18], 120°C baking for 48 hours [13], and “modified” 75/120°C baking [19, 20]. One of the nitrogen doped cavities has been studied with a step-by-step material removal after initial doping to directly probe the effect of gradual changes in interstitial nitrogen concentration on cavity performance.

All cavities have been first cooled down to 2 K where the standard measurements [21] of  $Q_0$  as a function of the accelerating gradient  $E_{\text{acc}}$  have been performed. Characteristic  $Q_0(E_{\text{acc}})$  curves obtained at 2 K are shown in Fig. 1.

Measurements of the resonant frequency  $f_0$  shift with temperature were performed as follows. All cavities were equipped with a number of resistance temperature detectors (RTDs) and placed in a large helium dewar. Once in the dewar, liquid helium was used to cool to 4.2 K. To initiate warming, heaters located at the bottom of the dewar were used to boil off the helium. Once evaporated, warm helium gas was flown to continue warming. This process allowed for a warming rate of  $< 0.1$  K/min, slow enough to ensure the thermalization of the cavity, as confirmed by the RTD readings. Resonant frequency was recorded with a vector network analyzer. Measurements persisted through the niobium superconducting transition temperature  $\sim 9.2$  K and well into the normal conducting state. After measurements, the data was corrected to account for variations in dewar gas pressure.

For each of the  $f_0(T)$  datasets, an effective mean free path  $\ell$  within the cavity surface layer has been obtained by converting the measured frequency shift with temperature near  $T_c$  into a shift in the magnetic field penetration depth  $\lambda(T)$  using Slater’s theorem [22] and fitting

based on the modified Halbritter routine [23], following the same technique outlined in [14].

Overall, we have studied the frequency response of 41 cavities with various impurity structures in the RF layer. Of these 41, we have found a clear dip in the resonant frequency just below the  $T_c$  in 22 nitrogen doped cavities, similar to the one shown in Fig. 2(b). For other treatments, four other characteristic behaviors, which we labeled “foot”, “bump”, “dip+bump”, and “standard”, have been observed. More details are provided in the Supplemental Material.

In order to investigate the dependence of the dip on the nitrogen concentration, one of the cavities subjected to 3/60 nitrogen doping underwent several sequential material removal steps of the RF surface *via* electropolishing, with RF measurements performed after each step. The material removal allowed to gradually decrease the concentration of N present in the RF layer, resulting in an increase in  $\ell$ . After the combined 30  $\mu\text{m}$  material removal, the cavity was bulk electropolished and re-processed with the 2/6 N-doping surface treatment. The  $Q_0(E_{\text{acc}})$  and  $f_0(T)$  results along with the corresponding material removal amounts and extracted electron mean free path values are presented in Fig. 2.

We observe that dilute and uniform concentrations of nitrogen (short  $\ell$ ) produce a characteristic increase in  $Q_0$  at higher  $E_{\text{acc}}$ , a suppression in  $T_c$ , and an anomalous frequency dip just before  $T_c$ . As nitrogen concentration gradually decreases with more material removal, these behaviors are gradually diminished. The  $Q_0$  behavior with field approaches that of the typical EP cavity presented in Fig. 1. Meanwhile, the dip magnitude diminishes as the transition temperature assumes the clean niobium value. After the electropolishing and 2/6 doping, which is known to produce a larger nitrogen concentration than 3/60 doping, the dip feature returns with a larger magnitude and larger  $T_c$  decrease.

Fig. 2(c) plots the dip magnitude and transition temperature against  $\ell$ . The dip magnitude decreases strongly (close to exponentially) with increasing  $\ell$  values. Moreover, the transition temperature follows a similar dependence, varying by  $\sim 120$  mK throughout the course of the study. These changes are in good agreement with previous studies on effects of nitrogen and oxygen on niobium  $T_c$  [24]. Our findings clearly show that a frequency dip and corresponding  $T_c$  suppression occur in the presence of uniform and dilute concentrations of nitrogen impurities and that the concentration of nitrogen serves as a major parameter in determining the extent of the phenomena. As the  $\ell$  gradually approaches clean limit values, the  $T_c$  suppression is diminished, and the dip phenomenon gradually evolves into the “standard” feature.

To study the effect of the cavity resonant frequency on the dip, four niobium cavities with  $f_0=650$  MHz, 1.3 GHz, 2.6 GHz, and 3.9 GHz were subjected to the same nitrogen doping surface treatment, producing a nomi-

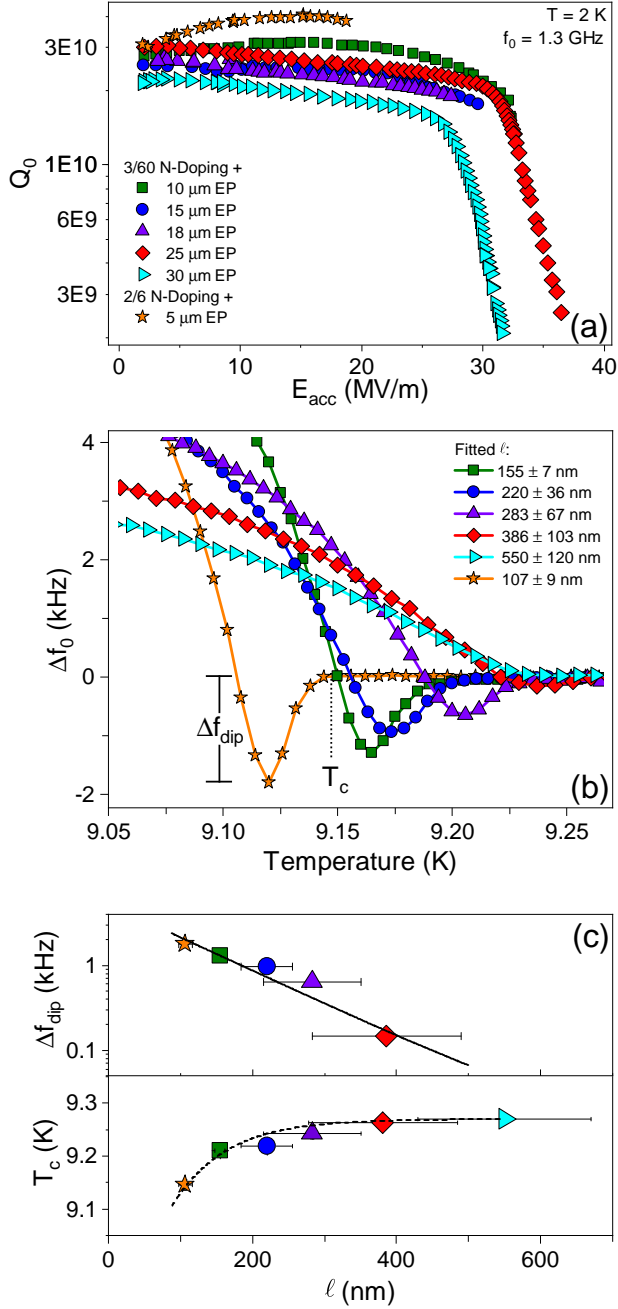


FIG. 2. (a) CW RF measurements and (b) resonant frequency response with temperature of a single 1.3 GHz Nb SRF cavity after sequential removal of the surface post nitrogen doping. The legend in (b) presents the fitted  $\ell$  in the RF layer after each step. Resonant frequency shift is reported relative to the normal conducting value near 10 K. The parameter  $\Delta f_{dip}$  is called the dip magnitude and  $T_c$  is defined here as the temperature at which the frequency shift becomes flat. (c) The magnitude of the dip and critical transition temperature are plotted against the fitted  $\ell$ . Horizontal error bars come from fitting while vertical error bars are smaller than the data points. Solid and dashed lines show  $e^{-\ell}$  and  $-e^{-\ell}$  relationships, respectively.

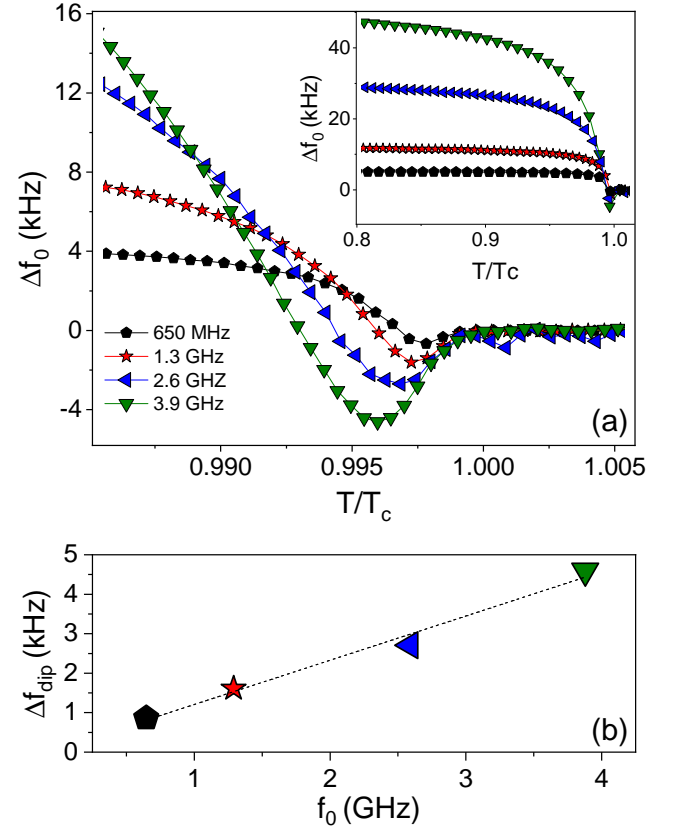


FIG. 3. (a) Frequency response with temperature of four cavities, each with different resonant frequency, processed to yield a nominally identical nitrogen concentration in the RF layer. Inset shows the response over a larger range of temperatures. (b) The dip magnitude plotted against the fundamental resonant frequency for each cavity. Dashed line shows a linear fit.

nally identical impurity structure in each cavity. The resulting  $f_0(T)$  curves are shown in Fig. 3(a). It is immediately observed that larger drive frequencies produce larger dip magnitudes. In fact, Fig. 3(b) shows that there is a linear relationship between these two parameters.

The linear trend observed in Fig. 3(b) has a positive correlation with the frequency dependence of the surface resistance shown in [12]. The authors of that paper attribute a stronger decrease in the temperature dependent resistance with field to non-equilibrium superconductivity, which may also play a role in the frequency behavior near  $T_c$ .

Lastly, to gain insight on the conditions under which different frequency features near  $T_c$  occur, we calculated the AC complex conductivity for two niobium cavities: i) the cavity presented in Fig. 2(a) with  $\ell = 550 \pm 120$  nm which showed the standard feature near  $T_c$  and ii) a nitrogen doped cavity that exhibited the prominent dip. The transition temperature of the latter cavity was 9.04 K; using Fig. 2(c), the extrapolated  $\ell$  was about 70 nm. Values of  $\sigma_1$  and  $\sigma_2$  have been obtained from  $Q_0(T)$  and

$f_0(T)$  data using the method discussed by Trunin [25]. We accounted for anomalous skin effects by using theory from Reuter and Sondheimer [26]. This method required the measurement of the surface impedance  $Z = R_s + iX_s$  for  $2 < T < 10$  K using the methods laid out in [27]. The calculated conductivities are presented in Fig. 4. As the technique used to measure the surface impedance sums over the inner surface, these curves represent the average response of the cavities. Further details on the technique are given in the Supplemental Material.

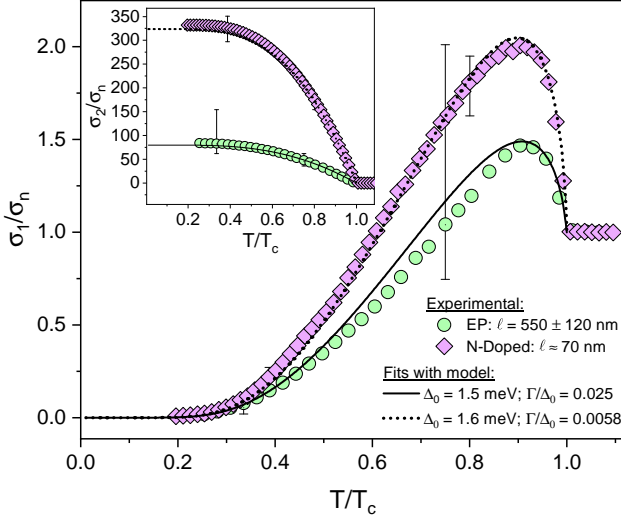


FIG. 4. Real ( $\sigma_1$ ) and imaginary ( $\sigma_2$ ) parts of the AC complex conductivity normalized to the normal conducting value  $\sigma_n$  of two 1.3 GHz cavities treated with electropolishing (EP) and N-doping. Error bars for the test post N-doping are dominated by uncertainty in the measurement while those shown post EP are dominated by error in fitted  $\ell$  value. Dashed and solid lines show fits with Eqs. 1-3.

From Fig. 4, we observe that both the EP and N-doped cavities exhibit the so-called coherence peak, with the maxima at  $\sim 0.9 T/T_c$  differing in amplitude. This suggests a variation in the quasiparticle behavior within the RF layer due to distinct impurity distributions.

The dashed and solid curves in Fig. 4 are calculated using a slightly modified version of the Mattis-Bardeen conductivity with the Dynes inelastic scattering parameter  $\Gamma$  [28] built in, given as

$$\frac{\sigma_1}{\sigma_n} = \frac{2}{\hbar\omega} \int_{\Delta}^{\infty} \frac{[f(E) - f(E + \hbar\omega)]g(E, \Gamma)}{\sqrt{(E + i\Gamma)^2 - \Delta^2}} dE + \frac{1}{\hbar\omega} \int_{\Delta - \hbar\omega}^{-\Delta} \frac{[1 - 2f(E + \hbar\omega)]g(E, \Gamma)}{\sqrt{(E + i\Gamma)^2 - \Delta^2}} dE, \quad (1)$$

$$\frac{\sigma_2}{\sigma_n} = \frac{2}{\hbar\omega} \int_{\Delta - \hbar\omega, -\Delta}^{\Delta} \frac{[1 - 2f(E + \hbar\omega)]g(E, \Gamma)}{\sqrt{(\Delta^2 - (E + i\Gamma)^2)}} dE, \quad (2)$$

$$g(E, \Gamma) = \frac{(E + i\Gamma)((E + i\Gamma) + \hbar\omega) + \Delta^2}{\sqrt{((E + i\Gamma) + \hbar\omega)^2 - \Delta^2}}. \quad (3)$$

Note the factor of 2 in Eq. 2. This simple phenomenological model gives a measure of the pair-breaking present in the RF surface by introducing subgap quasiparticle states and reproduces some of the salient features discussed in more rigorous theories at low  $\Gamma/\Delta_0$  values [29, 30].

From the fits, we find that both  $\sigma_1$  and  $\sigma_2$  of the EP cavity are best modelled with an average superconducting gap of  $\Delta_0 = 1.5$  meV and an inelastic scattering parameter of  $\Gamma/\Delta_0 = 0.025$ . The N-doped cavity is instead better fitted with a larger average superconducting gap of  $\Delta_0 = 1.6$  meV and a lower level of pair-breaking ( $\Gamma/\Delta_0 = 0.0058$ ).

These values are in good agreement with those obtained in point contact tunneling spectroscopy (PCTS) studies by Groll *et al.* on similarly treated cavity cutouts [31]. The N-doped samples in those studies showed more homogeneous  $\Delta_0$  values and lower levels of  $\Gamma/\Delta_0$  than those that came from EP cavities. This gives one possible cause for the difference in gap values obtained from the fits shown in Fig. 4; electropolished cavities contain localized defective regions that bring down the average superconducting gap. The lower level of pair-breaking observed in Fig. 4 for the N-doped cavity is likely due to the absence (or lower volume fraction) of proximity coupled nanohydrates and magnetic moments within the interface. This is consistent with the fact that N-doped cavities do not exhibit the high field  $Q$  slope caused by the proximity breakdown of hydrides at high fields [7, 10].

While PCTS reports lower values of  $\Gamma/\Delta_0$  for both N-doped and EP samples than what is shown in Fig. 4, this is likely due to differences in the probing depth between the two techniques. Since PCTS is more surface sensitive, it is likely that RF field measurements probe considerably deeper and sample regions with fewer pair-breaking mechanisms.

Although we focus primarily on the “dip” and “standard” features, it is likely that the three other frequency features near  $T_c$  follow some relationship with the mean free path, inelastic scattering, and the superconducting gap as well. This will be a topic of future study.

In this article, we have presented the first systematic studies of the anomalous resonant frequency behavior near  $T_c$  of bulk niobium superconducting radio-frequency cavities and showed the first observation of the coherence peak in these structures. Our findings open a new avenue for understanding the underlying physics behind the increase of the SRF cavity  $Q_0$  factor at higher fields in nitrogen doped cavities, suggesting the important role of the number of subgap quasiparticle states and the homogeneity of the superconducting order parameter. Furthermore, they provide previously unavailable direct superconducting state information for other modern cavity surface treatments. This new understanding can allow to further extend the obtainable quality factors in SRF cavities for accelerators, QIS, and fundamental physics

searches.

The authors would like to acknowledge O. Melnychuk and D. A. Sergatskov for technical support during measurements. Work supported by the Fermi National Accelerator Laboratory, managed and operated by Fermi Research Alliance, LLC under Contract No. DE-AC02-07CH11359 with the U.S. Department of Energy.

---

\* dbafia@fnal.gov

- [1] H. S. Padamsee, Annual Review of Nuclear and Particle Science **64**, 175 (2014).
- [2] A. Romanenko, R. Pilipenko, S. Zorzetti, D. Frolov, M. Awida, S. Belomestnykh, S. Posen, and A. Grassellino, Phys. Rev. Applied **13**, 034032 (2020).
- [3] R. Janish, V. Narayan, S. Rajendran, and P. Riggins, Phys. Rev. D **100**, 015036 (2019).
- [4] Z. Bogorad, A. Hook, Y. Kahn, and Y. Soreq, Phys. Rev. Lett. **123**, 021801 (2019).
- [5] A. Berlin, R. T. D'Agnolo, S. A. R. Ellis, C. Nantista, J. Neilson, P. Schuster, S. Tantawi, N. Toro, and K. Zhou, Journal of High Energy Physics **2020**, 88 (2020).
- [6] C. Gao and R. Harnik, arXiv:2011.01350 (2020).
- [7] A. Romanenko, F. Barkov, L. D. Cooley, and A. Grassellino, Superconductor Science and Technology **26**, 035003 (2013).
- [8] A. Romanenko, Y. Trenikhina, M. Martinello, D. Bafia, and A. Grassellino, in *Proceedings of the 19th International Conference on RF Superconductivity*, THP014 (2019).
- [9] A. Romanenko and D. I. Schuster, Phys. Rev. Lett. **119**, 264801 (2017).
- [10] A. Grassellino, A. Romanenko, D. Sergatskov, O. Melnychuk, Y. Trenikhina, A. Crawford, A. Rowe, M. Wong, T. Khabiboulline, and F. Barkov, Superconductor Science and Technology **26**, 102001 (2013).
- [11] D. C. Mattis and J. Bardeen, Phys. Rev. **111**, 412 (1958).
- [12] M. Martinello, M. Checchin, A. Romanenko, A. Grassellino, S. Aderhold, S. K. Chandrasekeran, O. Melnychuk, S. Posen, and D. A. Sergatskov, Phys. Rev. Lett. **121**, 224801 (2018).
- [13] H. Padamsee, *RF Superconductivity: Volume II: Science, Technology and Applications* (Wiley-VCH Verlag GmbH and Co., KGaA, Weinheim, 2009).
- [14] M. Martinello, A. Grassellino, M. Checchin, A. Romanenko, O. Melnychuk, D. A. Sergatskov, S. Posen, and J. F. Zasadzinski, Appl. Phys. Lett. **109**, 062601 (2016).
- [15] J. Bardeen, L. N. Cooper, and J. R. Schrieffer, Phys. Rev. **108**, 1175 (1957).
- [16] L. C. Hebel and C. P. Slichter, Phys. Rev. **113**, 1504 (1959).
- [17] B. Aune, R. Bandelmann, D. Bloess, B. Bonin, A. Bosotti, M. Champion, C. Crawford, G. Deppe, B. Dwersteg, D. A. Edwards, H. T. Edwards, M. Ferrario, M. Fouaidy, P.-D. Gall, A. Gamp, A. Gössel, J. Graber, D. Hubert, M. Hüning, M. Juillard, T. Junquera, H. Kaiser, G. Kreps, M. Kuchnir, R. Lange, M. Leenen, M. Liepe, L. Lilje, A. Matheisen, W.-D. Möller, A. Mosnier, H. Padamsee, C. Pagani, M. Pekeler, H.-B. Peters, O. Peters, D. Proch, K. Rehlich, D. Reschke, H. Safa, T. Schilcher, P. Schmüser, J. Sekutowicz, S. Simrock, W. Singer, M. Tigner, D. Trines, K. Twarowski, G. Weichert, J. Weisend, J. Wojtkiewicz, S. Wolff, and K. Zapfe, Phys. Rev. ST Accel. Beams **3**, 092001 (2000).
- [18] A. Grassellino, A. Romanenko, Y. Trenikhina, M. Checchin, M. Martinello, O. S. Melnychuk, S. Chandrasekeran, D. A. Sergatskov, S. Posen, A. C. Crawford, S. Aderhold, and D. Bice, Supercond. Sci. Tech. **30**, 094004 (2017).
- [19] A. Grassellino, A. Romanenko, D. Bice, O. Melnychuk, A. C. Crawford, S. Chandrasekeran, Z. Sung, D. A. Sergatskov, M. Checchin, S. Posen, M. Martinello, and G. Wu, arXiv:1806.09824 (2018).
- [20] D. Bafia, A. Grassellino, O. Melnychuk, A. Romanenko, Z.-H. Sung, and J. Zasadzinski, in *Proceedings of the 19th International Conference on RF Superconductivity*, TUP061 (2019).
- [21] O. Melnychuk, A. Grassellino, and A. Romanenko, Rev. Sci. Instrum. **85**, 124705 (2014).
- [22] J. C. Slater, Rev. Mod. Phys. **18**, 441 (1946).
- [23] J. Halbritter, Institut für Experimentelle Kernphysik (IEKP), Report No. KFK-Extern 03/70-06 (1970).
- [24] W. DeSorbo, Phys. Rev. **132**, 107 (1963).
- [25] M. R. Trunin, A. A. Zhukov, and A. T. Sokolov, Zh. Eksp. Teor. Fiz. **111**, 696 (1997).
- [26] G. E. H. Reuter and E. H. Sondheimer, Proceedings of the Royal Society of London. Series A. Mathematical and Physical Sciences **195**, 336 (1948).
- [27] D. Bafia, Ph.D. thesis, Illinois Institute of Technology (2020).
- [28] R. C. Dynes, V. Narayanamurti, and J. P. Garno, Phys. Rev. Lett. **41**, 1509 (1978).
- [29] T. Kubo and A. Gurevich, Phys. Rev. B **100**, 064522 (2019).
- [30] T. Kubo, Phys. Rev. Research **2**, 013302 (2020).
- [31] N. R. Groll, G. Ciovati, A. Grassellino, A. Romanenko, J. F. Zasadzinski, and T. Proslie, arXiv:1805.06359 (2018).

# Supplemental Material for ‘The Anomalous Resonant Frequency Variation of Microwave Superconducting Niobium Cavities Near $T_c$ ’

D. Bafia,<sup>1,\*</sup> A. Grassellino,<sup>1</sup> M. Checchin,<sup>1</sup> J. F. Zasadzinski,<sup>2</sup> and A. Romanenko<sup>1</sup>

<sup>1</sup>*Fermi National Accelerator Laboratory, Batavia, Illinois 60510, USA*

<sup>2</sup>*Department of Physics, Illinois Institute of Technology, Chicago, Illinois 60616, USA*

(Dated: July 8, 2022)

## FREQUENCY VS TEMPERATURE FEATURES

Fig. 1 shows the five resonant frequency variations just below the critical transition temperature ( $T_c$ ) in Nb SRF cavities. All five features have been observed while warming and cooling through  $T_c$ , which is expected as the superconducting phase transition is of the second order. The different features are characterized as follows. The “standard” feature shows a sharp transition of the resonant frequency to the normal conducting value. The “bump” feature, instead, shows a more gradual evolution of the frequency to the normal conducting value followed by a subsequent increase and decrease. A similar variation is observed for the “dip+bump” feature, but the resonant frequency shows a slight decrease before the subsequent behavior. A “foot” feature exhibits a frequency saturation before assuming the normal conducting value. Lastly, the “dip” feature shows a prominent decrease prior to full phase transition.

## CAVITY PROCESSING TECHNIQUES

All the cavities used in this study first underwent bulk electropolishing to remove  $\geq 120 \mu\text{m}$  of material. We used the five following final processing techniques to prepare the inner RF surface of our superconducting radio-frequency cavities:

- Electropolishing (EP): degas at  $800^\circ\text{C}$  in a vacuum better than  $10^{-7}$  Torr for 3 hours followed by a  $40 \mu\text{m}$  removal *via* electropolishing [1].
- Low temperature  $120^\circ\text{C}$  baking: degas at  $800^\circ\text{C}$  in vacuum for 3 hours followed by a  $40 \mu\text{m}$  removal *via* EP. The cavity is then assembled for testing, evacuated, and baked *in-situ* at  $120^\circ\text{C}$  for 48 hrs [2].
- $75/120^\circ\text{C}$  baking: degas at  $800^\circ\text{C}$  in vacuum for 3 hours followed by a  $40 \mu\text{m}$  removal *via* EP. The cavity is then assembled for testing, evacuated, and baked *in-situ* at  $75^\circ\text{C}$  for 4 hours followed by  $120^\circ\text{C}$  for 48 hrs [3, 4].
- Nitrogen infusion: after degassing at  $800^\circ\text{C}$  in vacuum for 3 hours, the temperature is lowered to  $120^\circ\text{C}$  and nitrogen at a partial pressure of

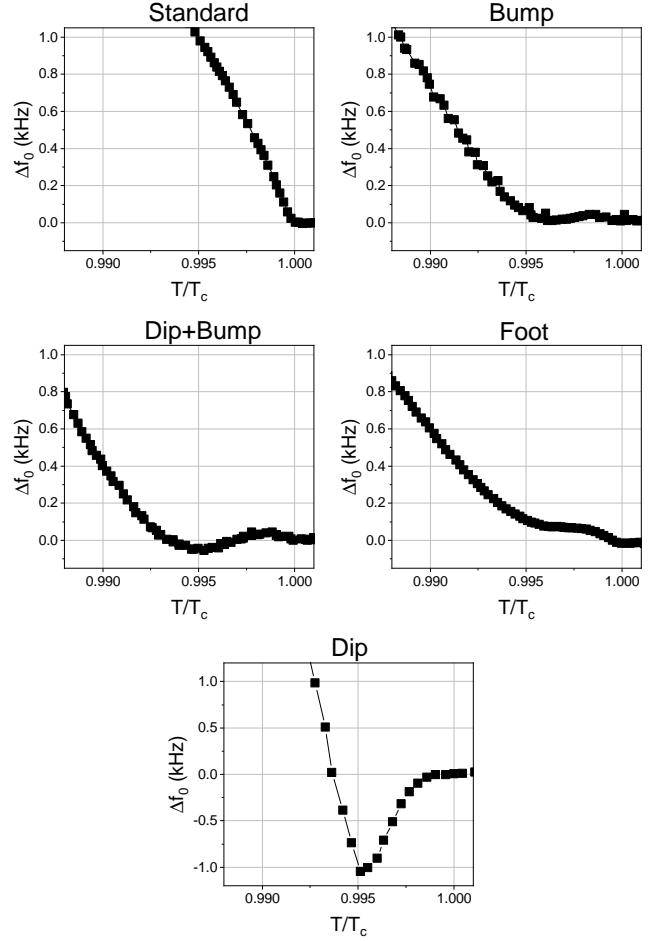


FIG. 1. Five observed resonant frequency variations of 1.3 GHz elliptical niobium SRF cavities near  $T_c$ .

$\sim 25$  mTorr is introduced into the furnace. The cavity is then annealed at  $120^\circ\text{C}$  in this nitrogen atmosphere for 48 hours [5].

- Nitrogen doping: degas at  $800^\circ\text{C}$  in vacuum for 3 hours. While maintaining this temperature, nitrogen gas is injected at a partial pressure of 25 mTorr for a duration ranging from 1 to 20 minutes. The nitrogen supply is then cut off and vacuum is re-established, annealing the cavity further for 0-60 minutes. After the furnace run, the first few micrometers of the inner surface are removed by EP to eliminate the niobium nitride phase precipitates,

leaving nitrogen to exist as interstitial extending for several micrometers inside the material [6]. The nitrogen doping recipes are usually referred to as “x/y doping”, where x is the duration in minutes of the annealing stage with nitrogen and y is the post-nitrogen vacuum annealing duration. For example, “2/6 doping” means 2 minutes of annealing with 25 mTorr of nitrogen gas followed by 6 minutes with nitrogen pumped out.

### EFFECT OF IMPURITY STRUCTURE ON FREQUENCY VARIATIONS NEAR $T_c$

A large ensemble of elliptical cavities was subjected to the treatments described in the previous section and tested using the methods laid out in the main text. The number of instances each feature in Fig. 1 occurred in resonant frequency shift data in the presence of a particular surface treatment was logged in Table I. We found that two of the electropolished cavities exhibited the standard feature while one showed the dip+bump feature. Both of the low temperature 120°C baked cavities exhibited the standard feature. The nitrogen infused cavities showed the foot, dip+bump, and standard features. The 75/120°C baked cavities revealed 4 out of the 5 behaviors near  $T_c$ , with the exception being the dip+bump. While a feature resembling a small dip was observed in one 75/120°C baked cavity, its magnitude of about 50 Hz was much smaller than what was observed for 22 doped cavities ( $\sim 1$  kHz). We believe this could have been a potential artifact of the helium pressure correction procedure. We note that 5 cavities exhibited a foot, suggesting that this behavior is characteristic of an oxygen enriched surface layer. All 22 nitrogen doped cavities investigated in this study exhibited a prominent dip in the resonant frequency.

	N-doped	N-Infused	75/120°C	120°C	EP
Dip	22		1 <sup>a</sup>		
Foot		1	5		
Bump			1		
Dip+Bump		2			1
Standard		1	3	2	2

<sup>a</sup>  $\Delta f_{dip} < 50$  Hz as compared to  $\sim 1$ -2 kHz in doped cavities, likely an artifact of the pressure correction

TABLE I. Occurrence of features in  $f_0(T)$  data near  $T_c$  for five typical SRF cavity surface treatments.

## CALCULATING CONDUCTIVITY

### Method

To calculate the complex conductivity, a method similar to the one laid out by Trunin was used [7]. The AC conductivity is given as

$$\sigma = \sigma_1 + i\sigma_2 = \omega\mu_0 \left( \frac{2R_s X_s}{(R_s^2 + X_s^2)^2} + i \frac{X_s^2 - R_s^2}{(R_s^2 + X_s^2)^2} \right), \quad (1)$$

where  $R_s$  and  $X_s$  are the surface resistance and reactance, respectively.  $R_s$  and  $X_s$  are given by

$$R_s(T) = \frac{G}{Q_0(T)} \quad (2)$$

and

$$X_s(T) = -2G \frac{\Delta f_0(T)}{f_0} + X_n. \quad (3)$$

where  $\Delta f_0(T)$  is the resonant frequency shift relative to the normal conducting value and  $f_0$  is the resonant frequency. The parameter  $G$  denotes the geometry factor. For the elliptical 1.3 GHz cavities studied here, this factor is 270  $\Omega$ .

To obtain the additive constant  $X_n$  in Eq. 3, the normal conducting surface resistance measured just above the transition temperature  $R_n(10 \text{ K})$  is required. In the local limit, valid for dirty Nb,  $R_n(10 \text{ K}) = X_n(10 \text{ K})$  is true. However, when the local limit is not applicable, as is true for high purity niobium [2], the anomalous skin effect must be considered. The correct relationship between  $R_s$  and  $X_s$  is obtained using the universal impedance curves plotted against the dimensionless parameter  $\alpha$  calculated by Reuter and Sondheimer in the microwave region [8]. The parameter  $\alpha$  is proportional to  $\ell^3/\rho\ell$ , where  $\ell$  is the mean free path,  $\rho$  is the resistivity, and  $\rho\ell$  is a temperature independent material constant, which is  $6 \times 10^{-16} \Omega\text{m}^2$  for Nb [2]. Thus, by knowing the  $\ell$ , it is possible to obtain  $X_n$ , which in turn yields the total reactance.

### Impedance Data

Fig. 2 shows the measured impedance data used to calculate the complex conductivities in Fig. 4 of the main text. Green circles and pink diamonds correspond to data acquired on EP and N-doped cavities, respectively. Data was acquired using methods laid out in [9]. Due to the change of signs in Eq. 3, a dip in frequency results in a peak in the reactance.

To ensure realistic values for the reactance, the experimental penetration depth at  $T = 0 \text{ K}$  was calculated via

$$X_{s,0} = \omega\mu_0\lambda_{0,\text{exp}} \quad (4)$$



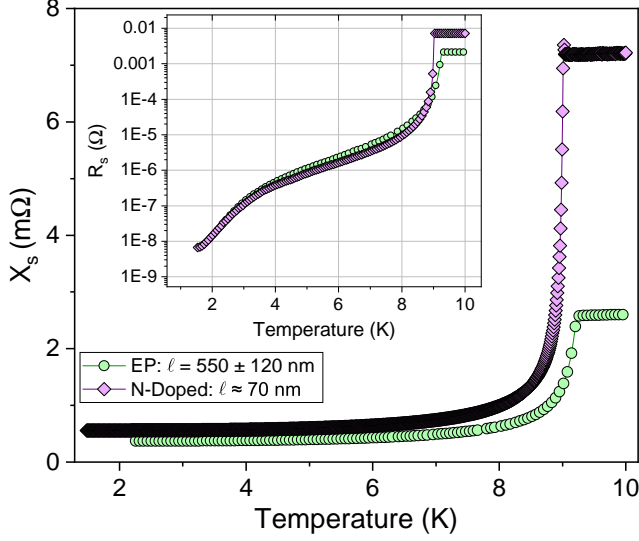


FIG. 2. Measured surface resistance and surface reactance of two 1.3 GHz cavities treated to either electropolishing (EP) or N-doping.

and compared with the effective penetration depth obtained from

$$\lambda_0 = \lambda_L \sqrt{1 + \frac{\xi_0}{\ell}}. \quad (5)$$

For Nb,  $\lambda_L = 39$  nm and  $\xi_0 = 38$  nm [10]. The experimental and calculated results shown in Table II are in good agreement.

Treatment	$X_{s,0}$ [ $\Omega$ ]	$\ell$ [nm]	$\lambda_{0,\text{exp}}$ [nm]	$\lambda_0$ [nm]
EP	$3.70 \times 10^{-4}$	550	$36 \pm 8$	40
N-Doped	$5.58 \times 10^{-4}$	70	$54 \pm 2$	48

TABLE II. Comparison of experimentally and theoretically obtained values for the penetration depth at  $T = 0$  K.

\* dbafia@fnal.gov

- [1] H. Padamsee, J. Knobloch, and T. Hays, *RF Superconductivity for Accelerators* (Wiley-VCH Verlag GmbH and Co., KGaA, Weinheim, 1998).
- [2] H. Padamsee, *RF Superconductivity: Volume II: Science, Technology, and Applications* (Wiley-VCH Verlag GmbH and Co., KGaA, Weinheim, 2009).
- [3] A. Grassellino, A. Romanenko, D. Bice, O. Melnychuk, A. C. Crawford, S. Chandrasekaran, Z. Sung, D. A. Sergatskov, M. Checchin, S. Posen, M. Martinello, and G. Wu, arXiv:1806.09824 (2018).
- [4] D. Bafia, A. Grassellino, O. Melnychuk, A. Romanenko, Z.-H. Sung, and J. Zasadzinski, in *Proceedings of the 19th International Conference on RF Superconductivity*, TUP061 (2019).
- [5] A. Grassellino, A. Romanenko, Y. Trenikhina, M. Checchin, M. Martinello, O. S. Melnychuk, S. Chandrasekaran, D. A. Sergatskov, S. Posen, A. C. Crawford, S. Aderhold, and D. Bice, *Supercond. Sci. Tech.* **30**, 094004 (2017).
- [6] A. Grassellino, A. Romanenko, D. Sergatskov, O. Melnychuk, Y. Trenikhina, A. Crawford, A. Rowe, M. Wong, T. Khabiboulline, and F. Barkov, *Superconductor Science and Technology* **26**, 102001 (2013).
- [7] M. R. Trunin, A. A. Zhukov, and A. T. Sokolov, *Zh. Eksp. Teor. Fiz.* **111**, 696 (1997).
- [8] G. E. H. Reuter and E. H. Sondheimer, *Proceedings of the Royal Society of London. Series A. Mathematical and Physical Sciences* **195**, 336 (1948).
- [9] D. Bafia, Ph.D. thesis, Illinois Institute of Technology (2020).
- [10] B. W. Maxfield and W. L. McLean, *Phys. Rev.* **139**, A1515 (1965).